DISCLAIMER

This report was prepared as an account of work sponsored by an agency of the United States Government. Neither the United States Government nor any agency thereof, nor any of their employees, makes any warranty, express or implied, or assumes any legal liability or responsibility for the accuracy, completeness, or usefulness of any information, apparatus, product, or process disclosed, or represents that its use would not infringe privately owned rights. Reference herein to any specific commercial product, process, or service by trade name, trademark, manufacturer, or otherwise does not necessarily constitute or imply its endorsement, recommendation, or favoring by the United States Government or any agency thereof. The views and opinions of authors expressed herein do not necessarily state or reflect those of the United States Government or any agency thereof. Reference herein to any social initiative (including but not limited to Diversity, Equity, and Inclusion (DEI); Community Benefits Plans (CBP); Justice 40; etc.) is made by the Author independent of any current requirement by the United States Government and does not constitute or imply endorsement, recommendation, or support by the United States Government or any agency thereof.

Final Technical Report – Down Select Report

Project Title: Low-Cost, High-Performance Carbon Fiber for Compressed Natural Gas Storage Tanks

Project Period of Performance: 10/1/2021 to 9/30/2023

Date of Report: 11/5/24

Recipient: University of Virginia

Technical Contact: Xiaodong (Chris) Li, xl3p@virginia.edu

Working Partners: Cytec Engineered Materials, Hexagon R&D LLC, ORNL, SRNL

Business Contact: Stephen Cornelison, sc6bt@virginia.edu

DOE Manager(s): Zeric Hulvey, zeric.hulvey@ee.doe.gov; Asha-Dee Celestine, Asha-Dee.Celestine@ee.doe.gov

Table of Contents

ACKNOWLEDGMENT:

This material is based upon work supported by the U.S. Department of Energy's Office of Energy Efficiency and Renewable Energy (EERE) under the Hydrogen and Fuel Cell Technologies Office (HFTO) Award Number DE-EE0009239.

DISCLAIMER:

Termination letter gave this context:

“We acknowledge receipt of the down-select report as the Final Technical Report.”

Executive Summary

The aim of this project is to reduce the cost of Type IV, carbon fiber (CF) composite overwrap compressed gas storage tanks by reducing the cost of CF and CF composites. The project team worked to reduce the cost of CF by exploring and testing opportunities for a low-cost alternative precursor material for CF production to supplant market-dominant and costly polyacrylonitrile (PAN). Concurrently, the team aimed to reduce the cost of the tanks at the composite level by improving the interfacial adhesion between the fibers and the matrix resin through the incorporation of low-cost nanoparticles recycled from waste materials, which would reduce the volume of costly CF required to achieve the same tank performance.

At the end of the first year, the project team selected mesophase pitch as the primary precursor candidate from a field of materials based on the superior mechanical performance and cost-saving potential. During the second year, the team produced CFs derived from mesophase pitch achieving an average tensile strength of 365.6 ksi and average tensile modulus of 40.74 Msi. Facility availability for spinning and converting these fibers at greater scale has hindered scale-up demonstration, but the team has identified opportunities to conduct this work in the near term. Cost modeling shows that these mesophase pitch-derived CFs can be up to 40% less expensive than PAN-derived CFs due to the lower cost of the feedstock material, higher throughput, greater conversion yield, and lower cost spinning method and compared to PAN.

Additionally, the team has demonstrated at lab-scale that nanoparticle coating CFs can significantly increase the interfacial shear strength and load transfer efficiency of CFs in a matrix. Single filament pull-out testing showed a 27% average increase in max interfacial shear strength due to this coating. A continuous method of applying these coatings to a tow of CF has been developed for scale-up. 26 m tows of coated CFs were produced using this system and formed into composite ring samples for ASTM ring burst testing. Issues with the testing protocol have limited assessment of these results.

A prototype Type IV tank was designed to meet ANSI HGV2 standards, and the design criteria set out by DOE, using the CF properties developed by the team paired with a proprietary resin matrix, a polyamide liner, and aluminum end bosses. The tank weighs 153.1 kg and with a total capacity of 5.8 kg H_2 (5.6 kg usable), which yields a gravimetric capacity of 1.17 kWh/kg. Cost modeling predicts that the tank will have a projected cost of $15.73/kWh. Tank performance modeling does not include considerations for fiber-matrix load transfer efficiency improvements offered by nanoparticle coating method.

The team's efforts over the course of this project have culminated in a final score of 3 points based on the DOE down-select scoring criteria. The leading candidate mesophase pitch-derived CF produced by the team scored 3 points from the rubric, earning 0 points each for the strength and modulus of the fibers and 3 points for projected cost. The prototype tank designed by the team scored 0 points from the rubric, earning 0 points based on projected cost, and 0 points for gravimetric capacity. Several pathways for continued development of the primary candidate fibers and composites are outlined in the final section of this report, and the project team is confident that all metrics can be improved in a short timeframe.

Project Introduction

The U.S. Department of Energy has identified hydrogen and compressed natural gas (CNG) as alternative vehicle fuels critical to achieving the greenhouse gas emission reductions required to meet the challenge of global climate change. These fuels require onboard storage at very high pressures in storage tanks. Several types of tanks have been developed to meet these constraints. More than 90% of the current CNG storage tank market consists of heavy, all-steel Type I tanks [1]. The remainder of the market consists of hybrid composite and metallic tanks, Type II-IV, or fully composite linerless tanks, Type V, that are extremely costly compared to Type I tanks. Heavy tanks limit the payload capacity of medium and heavy-duty vehicles, but the cost of lightweight tanks makes onboard hydrogen or CNG prohibitively expensive [2]. Low-cost, lightweight storage tanks are needed to enable broader adoption of hydrogen and CNG transporting and fueled medium and heavy-duty vehicles.

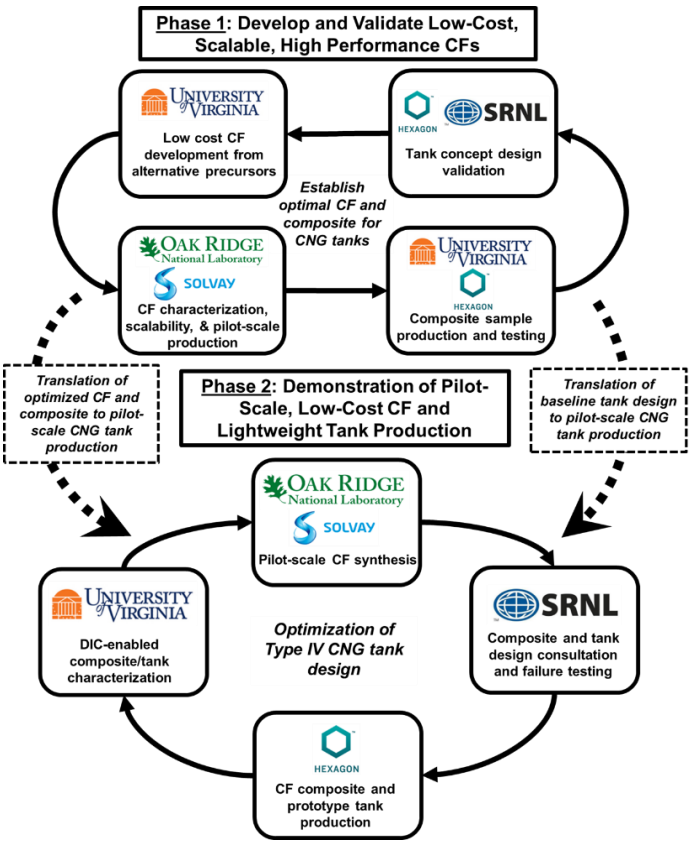

Figure 1. Project workflow.

Carbon fiber (CF) is an ideal material for lightweight composite tanks that meet the pressure and safety standards required of hydrogen and CNG storage tanks, but it is necessary to reduce the cost of CF, which can account for over half of the composite storage tank cost [3]. The high cost of CF is due to the high cost of its precursor material, PAN, and the precursor conversion process [4], so low-cost alternative precursors can significantly reduce cost. Herein, a team of experts in CF synthesis, CF composite production, CF-matrix interactions, CNG storage tank manufacturing, and pressure vessel testing has been assembled to conduct the research and development required to realize low-cost and lightweight hydrogen and CNG storage tanks, Figure 1.

Objectives

The project objectives are to design low-cost, lightweight, Type IV composite compressed gas storage tanks that meet ANSI HGV2 standards, and to establish a methodology for their scaled-up manufacturing. These objectives are divided into two phases (Phase 1: Years 1-2 and Phase 2: Years 3-5). In Phase 1, the team has developed methods for scalable production of low-cost, high-performance CF and for improving CF-matrix interfacial load transfer efficiency. In Phase 2, the scalability of the novel fibers from Phase 1 will be investigated and enhanced, and prototype hydrogen/CNG storage tanks will be produced from these fibers and composites.

Approach

The project team has worked toward achieving its objectives and the performance criteria set out by the DOE through parallel efforts to develop low-cost, high-performance CFs from alternative precursor materials and to enhance the interfacial properties of CF composites. Alternative precursor investigations began with a broad survey of opportunities, which were filtered down to one leading candidate based on mechanical performance and cost savings potential. Matrix-CF load transfer efficiency improvement was pursued through nanoparticle coating of the fibers, which was then demonstrated at pilot-scale to produce composite rings for burst testing. Through these two strategies the team could significantly reduce the cost of hydrogen and CNG storage tanks by reducing the cost and the volume of the CF used to make them. Accordingly, a prototype tank featuring the materials developed by the team was designed to demonstrate this potential.

Phase 1 Results

The results of the team's Phase 1 efforts are organized by project milestone as outlined in the Statement of Project Objectives.

Milestone 1.1 – Manufacture carbon fiber derived from low-cost precursors

To complete the first milestone of the project, the team surveyed a wide range of potential precursor materials including mesophase pitch, commodity polymers, a proprietary high-char polymer derived by Solvay, and blends of these materials in various combinations. This effort involved developing methods to spin the precursor fibers to minimal diameters and optimizing the conversion process to produce CF from these precursors. Broad spectrum characterization of the fibers at all stages from precursor to CF informed and accelerated subsequent iterations to maximize mechanical properties, and a novel displacement and strain tracking system and method was developed during the course of this work. At the end of year one, mesophase pitch was downselected from the field of alternative precursors for intensive development while limited development of other candidates continued to leverage cross-applicable discoveries. At the end of year two, mesophase pitch-derived CF achieved readiness for development at pilot-scale. The results of this work are elaborated in the following subsections organized by precursor material.

Low-cost displacement and strain detection using color tracking

A novel system of displacement and strain detection using optical image analysis was developed to assist in the characterization of the materials and processes developed during this project. A high-accuracy color tracking algorithm was developed and demonstrated using consumer-grade cameras for various applications. This system was used to track the shrinkage of ultra-high molecular weight polyethylene fibers during sulfonation, discussed below, and the tensile testing of single fibers during this project, and use cases extend well beyond these. US and international patent applications (PCT/US2024/41952) were filed for this system and method. A detailed description of this invention is included in Appendix A: System and method for displacement and strain detection using color tracking.

Mesophase pitch-derived carbon fibers

Mesophase pitch-derived CF has been commercialized for decades and represents approximately 10% of the global market [5]. They are constrained to this small share of the market by their lower ultimate strength compared to PAN-derived CF (≤ 4 GPa vs. ≤ 7 GPa), but their exceptional tensile modulus has earned many specialized applications [6–8]. Crucially, pitch is a significantly cheaper precursor material than PAN, as much as 82% cheaper per ton [9], and it is melt-processable, which is significantly cheaper with much greater throughput than the solution spinning required for PAN [5,10]. Thus, the team set out to unveil the process-structure-property mechanisms underlying mesophase pitch-derived CF production and to leverage this understanding to surpass current limits to mechanical properties thereby achieving high-performance, low-cost CF.

Over the course of the project, the team went through several iterations of development of mesophase pitch-derived CFs with a specific focus on producing CFs with high tensile strength. Three distinct generations of CF were produced with different tensile properties and microstructures. Upgrades to the equipment, spinning procedures, and conversion parameters improved tensile properties. Ultimately, fine control of the CF microstructure was achieved. The tensile properties of all three generations of CFs are presented in Table 1. Here, the terms “type 1” and “type 2” refer to the different microstructures the team was able to induce in the Generation 3 CFs.

Table 1. Maximum mechanical properties of the mesophase pitch-derived carbon fibers obtained throughout the course of the project.

	Tensile modulus GPa (Msi)	Tensile strength GPa (ksi)	Tensile strain, %
Generation 1	149 (22)	1.25 (181)	0.90
Generation 2	219 (32)	2.75 (399)	1.30
Generation 3 (type 1)	380 (55)	2.50 (363)	0.70
Generation 3 (type 2)	374 (54)	3.34 (484)	0.92

The team found that the fiber spinning process was as important to the development of mechanical properties as the subsequent thermal treatments. Therefore, the improvements in fiber spinning will be discussed first, followed by a discussion of optimizing the stabilization and carbonization steps of CF production.

Mesophase Pitch-CF Precursor Fiber Spinning Developments

Generation 1 CFs represent the team’s initial attempt at mesophase pitch-based CF production. A custom pressure driven “one shot” melt extruder was designed and fabricated to produce mesophase pitch precursor fibers. The CFs derived from these precursor fibers were of large diameter, > 10 μm, and exhibited macroscale pores, > 500 nm, lack of directional texture, and evidence of melting in the fiber core resulting from incomplete stabilization of the fiber center. Consequently, the fibers’ mechanical properties were poor. This initial trial highlighted many opportunities for process improvements.

Processing upgrades resulted in a step change in precursor fiber quality and structure and CF properties, which are referred to as Generation 2. These new fibers featured

much smaller diameters and large striations on the fiber surface indicating good alignment of the carbon crystallites with the fiber axis. The smaller diameter of these fibers enabled complete stabilization. However, some surface defects were observed, which can decrease tensile strength [11], indicating that the spinnerets were of low quality.

Following Generation 2, the melt spinning system was scaled down for faster heating and cooling and a through-wall thermocouple was added to measure the temperature of the melt. Commercial-grade spinnerets were adapted into the design to further improve the extrusion flow characteristics. This and several other updates yielded yet another step change in fiber quality, and the resulting CFs were designated Generation 3. Many of the surface defects seen in Generation 2 fibers were no longer observable in Generation 3 fibers. A major achievement of Generation 3 CFs was the precise control of the attained microstructure.

To evaluate the mechanical properties of the Generation 3 fibers in a composite, the CFs were formed into a unidirectional composite with a volume fraction between 55-58 % resin for mechanical testing, Figure 2a.

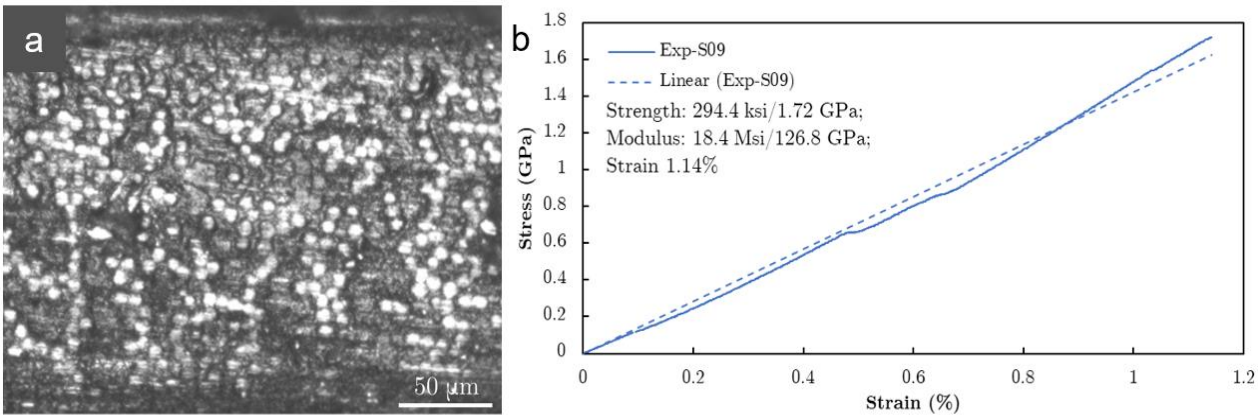

Figure 2. (a) Optical microscope image of cross-section of composite produced with random microstructure mesophase pitch-derived CF and (b) resultant tensile properties.

The composite was formed into a uniaxial tensile sample with a rectangular cross-sectional area. The composite was pulled in tension until failure, and the resulting stress strain curve is shown in Figure 2b. These properties represent the modulus and strength of a composite that can be manufactured with the UVA CFs and an epoxy resin (West Systems 105 epoxy resin). The composite properties could be further improved by improving the CF volume fraction, CF properties, or CF surface treatment [12].

Mesophase Pitch-CF Stabilization and Carbonization Developments

The mechanisms of oxidative stabilization of mesophase pitch were studied to optimize the stabilization process for cost and CF mechanical performance. Through variation of the oxidation temperature and hold time, a range of fibers with different oxygen concentrations and take up methods were created. These fibers were subsequently carbonized with the resulting CFs possessing a large range of mechanical properties. An optimized procedure was discovered and followed for all mesophase pitch fiber production as a result . Greater detail on this study is published in [13].

Contamination

The mesophase pitch-derived CF produced in the lab at UVA was susceptible to deleterious contamination during batch carbonization. The team worked diligently to mitigate the contamination which resulted in significantly improved mechanical properties. Mitigation strategies learned during this process will be translated to scaled production to accelerate the development of high-performance CF derived from mesophase pitch. Long lead times to acquire ultra-high purity furnace tubes and long repair times for the furnace available at UVA has delayed progress in further eradicating contamination. Encouragingly, these non-technical limitations can be overcome in a short time and the tensile properties are expected to increase substantially afterwards.

Commodity polymer-derived carbon fibers

Commodity polymers such as polyethylene and nylon have received great attention as potential alternative precursor materials for CF production because they are plentiful and cheap due to their ability to be melt spun, as compared to the costly wet spinning process required for PAN [14]. The project team reviewed an array of commodity polymers for new opportunities for alternative precursor development and chose to advance polyethylene and nylon to lab-scale trials. Neither precursor was the leading candidate at the downselection point, but the team's effort produced important insights that are described in brief below.

Polyethylene

Polyethylene has captured the attention of research and development teams as a potential low-cost precursor of CFs for decades, and significant progress has been made towards producing CFs with functional mechanical properties [15]. Across several works published in the 1990s, Zhang and his co-authors [16–18] showed that ultra-high molecular weight polyethylene (UHMWPE)-derived CFs could achieve high mechanical properties and suggested that further work could be done to enhance these properties. Accordingly, the project team hypothesized that the high molecular alignment of this precursor paired with conversion parameter optimization may yield CFs with sufficient mechanical performance to achieve the project target goals. Considering the high cost of contemporary commercially produced UHMWPE, this exploration was bifurcated into parallel pursuits of: 1) optimizing the conversion of commercially available UHMWPE, and 2) developing low-cost UHMWPE via fiber spinning process optimizations and nanocomposite development.

1) UHMWPE conversion optimization

Tension applied during the sulfonation-stabilization of UHMWPE was selected as the first parametric optimization of the UHMWPE conversion process based on the conclusions made by Zhang and Bhat [17]. Dyneema SK60 UHMWPE fibers with a nominal average diameter of 12 μm were selected for this study. A custom apparatus was designed to apply deadweight tension to the precursor fibers immersed in high concentration sulfuric acid, Figure 3. Complete stabilization was identified via differential scanning calorimetry (DSC), TGA, and SEM of carbonized fibers.

A log-sweep of applied tension was conducted and the stabilized fibers were carbonized in an argon atmosphere. Polyethylene fibers are known to shrink significantly during the

sulfonation process, but applied tension can mitigate this effect. The results showed significant improvement in the morphology of the fibers with increasing sulfonation tension.

Raman spectroscopy and XRD were employed to probe the microstructural evolution of the fibers with respect to tension applied during sulfonation stabilization. The results show that maximizing tension is crucial to developing larger and better aligned crystallites, which is crucial to the development of fiber mechanical properties. Single-filament tensile testing corroborated the conclusions made by Raman and XRD analysis; Ultimate tensile strength and Young's modulus increased significantly with increasing applied sulfonation tension . Greater detail on this study is published in [19].

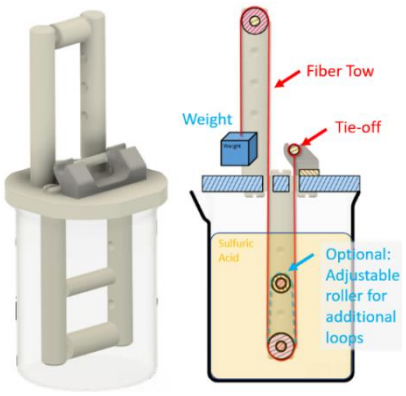

Figure 3. CAD rendering and cutaway schematic of a deadweight tensioning apparatus for the sulfonation stabilization treatment of polyethylene fibers.

2) Low-cost UHMWPE precursor

The high cost of UHMWPE necessitates the exploration of cost-reduction for consideration as a low-cost precursor material for CF production. Two approaches were considered by the project team: 1) utilizing low-cost nanoparticles to form high-performance UHMWPE nanocomposites that require less processing to achieve the same mechanical performance, and 2) replacing the toxic, and consequently costly, solvents used in the UHMWPE gel spinning process with ecologically friendly alternatives. The former opportunity was prioritized over the latter and is discussed in detail below. The project team thus designed and fabricated a lab-scale ram extruder monofilament gel spinning system for rapid iteration through gel and spinning parameters, Figure 4.

Pure UHMWPE and UHMWPE nanocomposite fibers were fabricated to compare the mechanical properties, surface morphology, and crystal structure development associated with the incorporation of nanoparticles. UHMWPE was blended with nanoparticles at different wt. %. The gel solution was fed into a stainless-steel syringe and extruded into a filament at a high temperature. Single-filament tensile testing revealed that the addition of nanoparticles could lead to an increase in the tensile strength of the fibers.

These lab-spun UHMWPE fibers were then converted into CFs using the same sulfonation-stabilization and carbonization. The fibers were often brittle and/or fused together, but a small sample size was suitable for single-filament tensile testing. Further optimization of spinning process parameters, nanoparticle concentration, parameters of sulfonation and carbonization is necessary to enhance the mechanical performance of CF derived from UHMWPE composite precursor fibers.

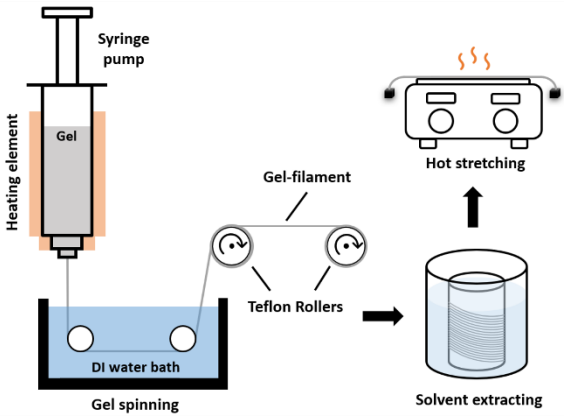

Figure 4. Schematic of gel spinning process.

Nylon (PA6)

Polyamide 6, tradename Nylon® and often abbreviated to PA6, has been recently demonstrated as a potential low-cost alternative CF precursor [5,20–23]. The published mechanical properties of PA6-derived CF are low relative to the targets set out in this project, but the team explored opportunities to enhance these properties including incorporating nanoadditives into the precursor fibers and increasing molecular alignment via stretching of the precursor fibers. Extensive work to determine optimal nanoadditive loading and dispersion optimization was required, but limited access to twin-screw extrusion made this infeasible. The team's focus then shifted to precursor stretching.

Precursor fiber stretching during formation and applied tension during conversion are crucial to the development of mechanical properties in PAN-derived CF production [24]. So, the team applied this insight to PA6 via physical stretching of the as-spun precursor fibers. The fibers were stretched in increments to observe the effect on size, crystallinity, surface roughness, and mechanical properties. After stretching, the samples were mechanically tested to failure to determine the differences between stretched and unstretched responses. The results from the stretching revealed an altered stress strain response due to the amount stretched.

Single-crystal XRD was used to explore the effect of stretching on the fiber microstructure. The fact that stretching causes a more disordered semicrystalline state is a negative indicator for improving the performance of PA6-derived CF. These effects did not translate into higher tensile properties of the CF, so PA6 was not studied further. Greater detail of this study can be found in [25].

Blended pitch-commodity polymer-derived carbon fibers

The team explored blending mesophase pitch and commodity polymers in an attempt to "trade" the above-target modulus of mesophase pitch-derived CF for increased tensile strength and strain to failure. Two types of melt-spinnable polymers were employed for this purpose: linear low-density polyethylene (LLDPE) and polyethylene terephthalate (PET). PET showed better dispersion within mesophase pitch than LLDPE, but neither blend could achieve the target properties by the downselection point. Greater detail on the team's efforts with these blends are available in two associated publications [26,27].

Pitch/LLDPE blends

Blends of LLDPE and mesophase pitch were created using a simple dry-state mixing method (powdering and grinding) at varying LLDPE concentrations. These blends were spun into precursor fibers using a one-shot, batch extruder. Fiber diameters and spinning conditions were kept constant throughout the study to reduce their effect on the resultant fiber mechanical properties.

This two-phase behavior was confirmed via SEM of the fiber cross sections following single-filament tensile testing of the blended precursor fibers. Accordingly, the stress-strain curves from the tensile tests reflected this two-phase behavior. These blended precursors were then converted to CFs per the procedure established for pure mesophase pitch precursors at low carbonization temperature, and single-filament tensile tested to evaluate their mechanical properties. The results showed that the inclusion of LLDPE had a deleterious effect on fiber mechanical properties.

Pitch/PET blends

The compatibility and melt processibility of blended PET and lignin [28–32] inspired blending PET with mesophase pitch. PET and mesophase pitch were blended at varying PET weight percentages and spun into fibers by the same method as the LLDPE/pitch blends.

Fibers produced from one blend showed the most promise as a CF precursor and were therefore oxidized and carbonized. The carbonized fibers were mechanically tested, and the CFs produced from this blend are now stiffer than pure pitch CFs, showing an increase in the modulus and a decrease in strain, which is the inverse of the relationship for the precursor fibers.

Pitch/Polyamide 6 Blends

Blending of various pitches and PA6 was attempted at ORNL. Four different pitches were explored due to their drastically different molecular structures, which could have an impact on their miscibility with PA6. Typically, the molecular components of petroleum-based pitches are known to be more aliphatic, with pending methyl or ethyl groups and bridges between aromatic rings, as compared to coal tar-based pitches which molecular components are very condensed, very aromatic. Also, the difference in molecular weight distribution and in crystallinity between isotropic and mesophase pitches is another factor that could influence the molecular interactions between the pitch molecular components and the PA6 chains leading to potential differences in miscibility. However, none of the blends exhibited complete miscibility between the pitch and polyamide, Figure 5. More fundamental work is needed to modify the interactions between the pitch molecular components and the PA6 chains, but the project team decided to focus resources on more promising options.

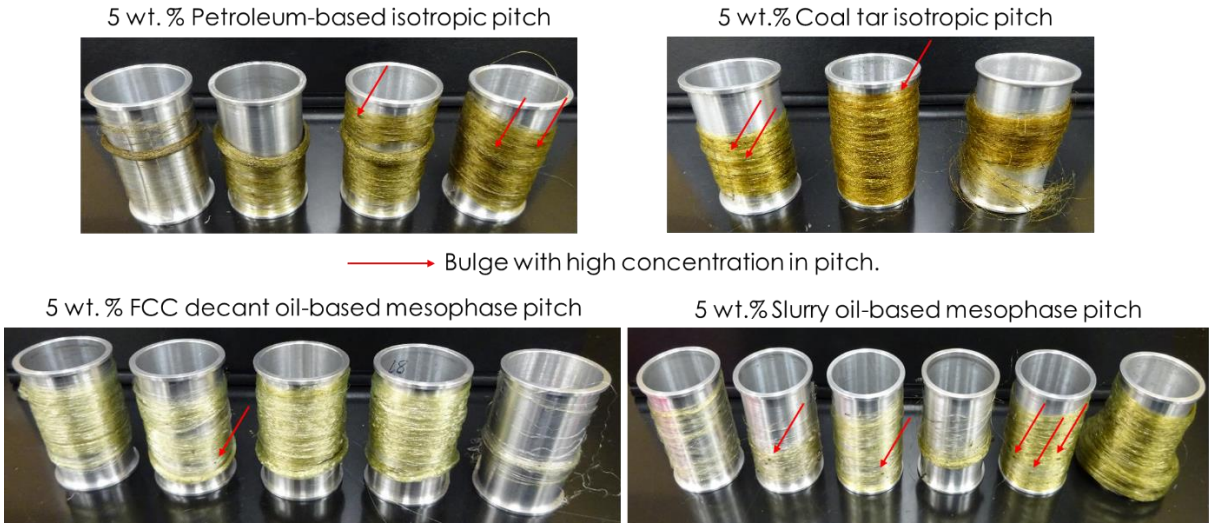

Figure 5. Macroscale pictures of pitch/polyamide-6 blended fibers spools.

Solvay polymer-derived carbon fibers

During the precursor exploration phase, Solvay presented a proprietary, melt processable polymer as a possible candidate. The polymer possesses a superior char yield compared to PAN, as well as a melt transition temperature that is well below its decomposition

temperature, which are key characteristics for producing CF. Viscosity measurements and initial melt-spinning trials at Solvay determined that it could be melt-spun into fibers. To enhance the stabilization and carbonization process, the polymer was blended with a reactive filler. This combination facilitated crosslinking and enabled shape retention at high temperatures.

UVA performed initial melt extrusion trials of the blend through a screw extruder using large-diameter spinnerets with a small number of holes, showing that the viscosity was appropriate for drawing into fibers. SEM images of the blended precursor fibers are shown in Figure 6. The images show an unusual nanostructured interior, which gave the fibers impressive workability and tenacity. Given these promising results, the team proceeded with a pilot-scale multi-filament melt-spinning trial of these blends to evaluate scale-up potential, which is further discussed in Milestone 1.3.

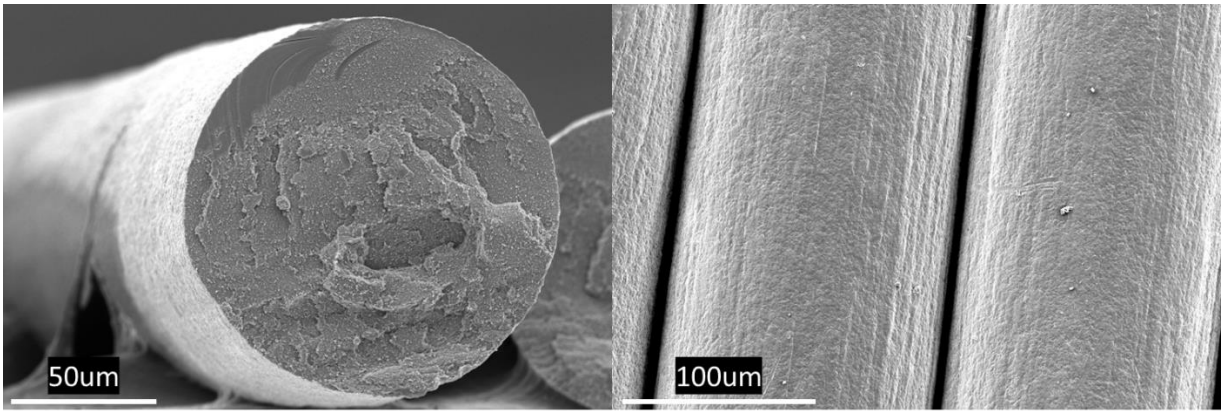

Figure 6. SEM images of the polymer and reactive filler blend precursor fibers.

Precursor down-selection summary

Mesophase pitch was selected at the end of the first year of the project for extensive development based on its superior mechanical properties, which approached or exceeded the targets set out at the beginning of the project. Mesophase pitch-derived CF is the primary candidate put forth by the team for a low-cost, high-performance CF capable of use in the construction of hydrogen storage tanks. The Solvay high-char polymer + reactive filler remains a high-potential secondary candidate that is only limited by material availability at the writing of this report. All other candidates failed to achieve mechanical properties meriting further development but still provided crucial insights.

Milestone 1.2 – Improve fiber load transfer efficiency

The team explored nanoparticle coatings of CF to improve the load transfer efficiency between the fibers and matrix in CF composites thereby reducing the CF volume, and thus cost, required to achieve the same tank performance. Specifically, the team focused on facile nanoparticle application methods and nanoparticles that can be derived from recycled materials via low-cost methods to maintain a low overall cost for the composites. The team began with lab scale coating techniques to apply nanoparticles onto the surface of commercial grade CFs. Single filament pullout testing in conjunction with four-point bending tests demonstrated the potential of these nanoparticles to improve the fiber load transfer efficiency within a resin matrix. This coating method was scaled-up to apply the coating to continuous tows of CF for ASTM ring burst testing.

Lab-scale fiber coating

Preliminary results focused on a simple coating method, referred to as one-step dipping, to demonstrate the effectiveness of low-cost nanoparticle coating techniques. Nanoparticles were added to a solution and shear mixed to achieve an even dispersion. Short lengths of CF were submerged in the suspension for one minute and allowed to fully dry prior to characterization. The CF was nanoparticle-coated as delivered and with the commercial sizing removed to assess the effect of the as-delivered sizing on the nanoparticle application.

Single filament pullout testing method

Single filament pullout testing was chosen to assess the effect of the nanoparticle-based coating on fiber-matrix load transfer efficiency. This mechanical testing procedure is widely used to quantify the interfacial shear stress (IFSS) required to achieve debonding at the interface between CF and epoxy samples. This test demonstrates the failure mechanics of fiber-reinforced composite materials through interfacial bonding strength and coefficient of friction driving interaction between fiber and epoxy [33]. Previous publications have shown a decrease in the coefficient of friction over the course of the pullout test due to interfacial friction reduction resulting in changes in surface roughness at the fiber/matrix interface [34]. It is hypothesized that the static friction coefficient dominates interfacial interaction during the early stages of pullout testing but changes in the surface roughness profile due to crack propagation and growth throughout the test result in the dynamic friction coefficient dominating the interfacial interaction during later stages of pullout testing.

After the conclusion of the single fiber pullout test, interfacial shear strength was calculated using Equation 1.

$$\tau_{Max} = \frac{F_{Fiber}}{\pi * \ l_e * D_{Fiber}} \quad (1)$$

where τ_{Max} is the maximum IFSS between fiber and epoxy matrix, F_{Fiber} is the maximum load recorded during the pull-out test, l_e is the length of fiber embedded in the epoxy matrix, and D_{Fiber} is the diameter of the fiber.

Single filament pullout testing results

Thirty successful tests were conducted for each sample designation: commercially sized and uncoated, unsized and uncoated, commercially sized and nanoparticle coated, and unsized and nanoparticle coated. The unsized and nanoparticle coated samples were conducted to quantify enhancements of interfacial properties from mechanical interlocking by removing any reinforcing effects offered by the commercial sizing. A considerable increase in IFSS at failure was observed in nanoparticle coated samples with and without the commercial sizing applied to the CFs. The average IFSS in nanoparticle coated samples with the commercial sizing intact was 27% greater than their uncoated counterparts.

Cohesive Zone Modeling

A linear cohesive zone model (CZM) with applicable traction separation law was developed using the Mechanical APDL solver package in Ansys 2023 R1 to better

understand the failure mechanics driving interfacial failure during single filament pull out testing. Previous publications have demonstrated the effectiveness of finite element analysis to create detailed CZMs to characterize fiber/matrix interaction during pullout testing [35–38]. A 2-dimensional axisymmetric model of single filament adhesion testing was built using the pure penalty CZM formulation criterion across the CZM interface. While the primary failure mechanism was mode 2 shear at the interface, the model was built to accommodate mixed mode failure for completeness.

The model was validated against experimental results for a variety of embedded lengths and nanoparticle coating conditions. The CZM model agreed well with the experimental results for all cases and performed better in cases with longer embedded lengths. The similarity between the experimental and CZM model results shows that the nanoparticle coating performed significantly better than the uncoated samples.

Four-point bend testing

The promising single-filament results encouraged the team to attempt this one-step dipping method to a tow of fibers. These tows were then used to manufacture composite bars with different resin systems. To test the different sizing treatments, fibers sized with UVA's nanoparticle coating version 1 (v1) and version 2 (v2) were combined with two different resin systems. The mechanical properties of the composite bars were evaluated via 4-point bending tests with digital image correlation (DIC). Load transfer efficiency was quantified by using the rule of mixtures, Equation 2.

$$E_{composite} = \eta * V_{fiber} * E_{fiber} + \left(1 - V_{fiber}\right) * E_{Epoxy} \quad (2)$$

The nanoparticle coating led to an increase in load transfer efficiency of the composites. Coating v1 yielded a 61% increase in load transfer efficiency over the untreated samples while coating v2 yielded a 90% increase in load transfer efficiency over the untreated samples. Mechanical results from 4-point bend testing on composites made by Hexagon showed a 16% increase in load transfer efficiency % for the v1 surface treated specimens over the untreated specimens. DIC was used during 4-point bend testing to characterize the degree of strain on the composites, Figure 7. The composites treated with both versions of the nanoparticle coating showed considerably less deformation, quantified by ε_2 strain, than their untreated counterparts. Ultimately, the

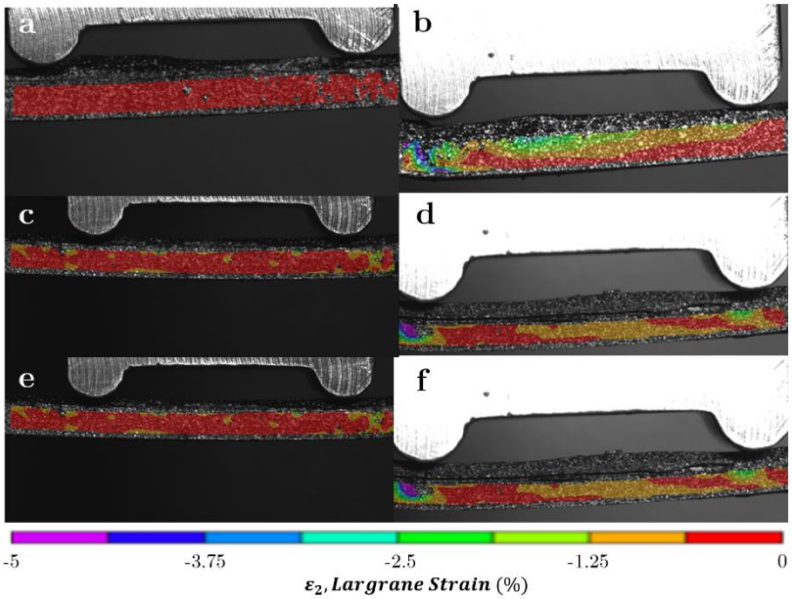

Figure 7. DIC analysis of 4-point bend testing with commercial CF and Bondo resin matrix where the fibers are: (a) treated with sizing v1, (b) untreated, (c) treated with sizing v2, (d) untreated. DIC analysis of 4-point bend testing with Zoltek fibers and Hexagon's resin matrix where the fibers are: (e) treated with sizing v1, (f) untreated.

load transfer efficiency calculations and strain measurements correlate well and match the results from single-filament pull-out testing, indicating that the nanoparticle coatings make a significant impact on CF-matrix interfacial properties.

Pilot-scale fiber coating application

Encouraged by the results of one-step dip coating of nanoparticles onto CF, the project team proceeded to scale-up the nanoparticle application to a continuous multifilament tow application method. The team leveraged its in-house, continuous tow bath treatment system capable of pilot-scale spool-to-spool tow applications [39]. The bath line fits within the footprint of a laboratory fume hood and features a payout spool, multiple rollers and baths with gaseous and liquid application nozzles, and a variable speed takeup winder. Electrophoretic deposition (EPD) was used to coat the fibers of a 50k CF tow with nanoparticles as has been applied in previous studies [40–42]. The pilot-scale EPD process was iteratively improved over several ‘generations’, using qualitative SEM and the later-discussed ASTM ring testing as a feedback metric. Apart from tuning process parameters, including electric bias magnitude, residence time of the tow in the treatment bath, and solution concentration, several significant improvements were made to the setup.

ASTM ring testing

The 26 m long surface treated tows produced using the pilot-scale bath line were shipped to Hexagon for ASTM ring burst testing. Composite ASTM rings were produced via filament winding and then subjected to burst testing using Hexagon's standard hydrostatic ring burst test. This test is intended to function as a sub-component screening method to evaluate the performance of materials in a loading scenario akin to a pressure vessel. Nanoparticle coatings were applied to CF tows as delivered from the manufacturer; The manufacturer-applied sizing was not removed. A 20.0% increase in median burst strength among control samples and a 15.7% increase in coated samples has been observed between the first and most recent (fourth) generations. While the increase in control performance may be partially attributable to small improvements in roller smoothness, it is more likely indicative of systematic changes in the ring testing protocol. Whether or not these changes have also biased the treated samples remains unknown.

After completion of ASTM ring testing by Hexagon, the fractured ring specimens were collected and shipped back to UVA for in-depth failure analysis via SEM/EDS. Characterization showed that delamination at the fiber/epoxy interface was the primary mode of failure in surface-treated and control samples. Characteristics of the fiber transfer line and ring sample formation method played a significant role in the test results. During ASTM ring winding of Gen1 and Gen2 samples, a significant amount of fuzzing (fibers fraying away from the tow due to friction) was observed on the treated fiber samples. Fiber fuzzing was also observed for the control samples but to a lesser degree. Both showed greater amounts of fuzzing than is typically observed during processing of T700 fiber. This fuzzing was mitigated for Gen3 with the usage of smoother rollers in the bath line designed to reduce sliding friction. Several modifications to the ASTM ring test methodology were required to account for the use of a 50k filament tow, including a reduction in the number of hoop layers used to fabricate the composite rings and modulating fiber volume fraction. Additionally, not all fibers in the tow were oriented

properly in the sample due to the size of the tow. Therefore, not all of the fibers contributed to the loading, which is a negative factor in the load transfer efficiency.

Milestone 1.3 – Demonstrate initial scalability

The scalability of the candidate CFs developed by the team was evaluated in the lab and at pilot-scale. In the lab, monofilament spinning was extended to multi-filament spinning to assess the ability to spin tows of the candidate precursor fibers. At UVA, a custom multi-hole spin pack compatible with a lab-scale screw extruder was designed and manufactured to gain insights and identify challenges before attempting spinning at a pilot-scale facility, and to replicate and resolve challenges identified at the pilot-scale facility. In the latter case, filament breakage inhibited the production of multi-filament tows at the pilot-scale facility, and the team was able to demonstrate a method of continuous multifilament spinning enabled by spraying a lubricant on the fibers before takeup, Figure 8. This insight will be transferred to subsequent pilot-scale spin trials.

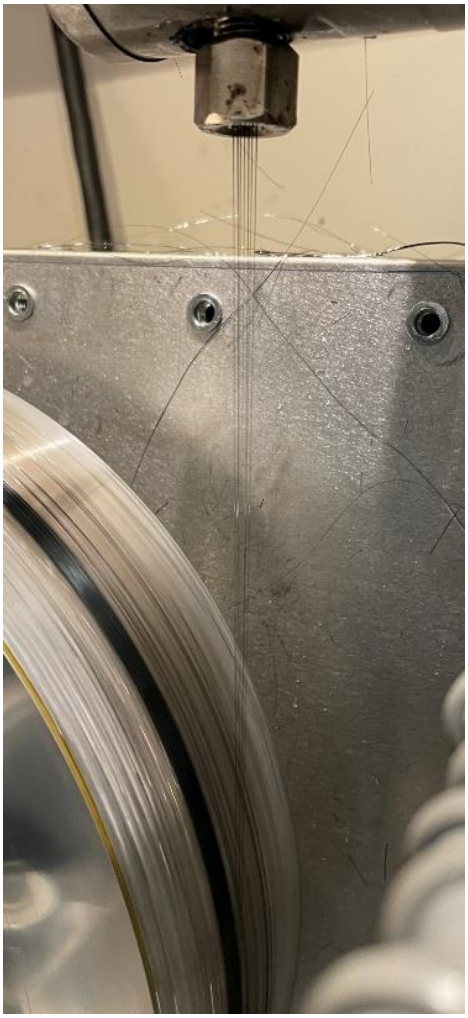

Figure 8. Lab-scale multi-filament spinning of pitch precursor tows. 7 filaments are simultaneously taken up onto a winder.

At the pilot-scale, Solvay produced melt-spun fibers using their blended precursor material comprised of high-char polymer and reactive filler that had previously undergone evaluation in a smaller lab-scale extrusion set-up. Based on their viscosity and thermal characteristics, two primary blend ratios were identified as promising candidates for conversion into CF. Batches of precursor fiber tows, each consisting of 19 filaments and over 100 meters in length, were produced from both types of blended precursor materials. The choice of 19 filaments was influenced by equipment and material availability constraints. The material performed well during this process, and it is anticipated that scaling up to 100 or even 1000+ filament spinning would present minimal challenges. Importantly, these precursor fiber tows exhibited sufficient tenacity to be processed on conventional PAN oxidation and carbonization lines.

The precursor fibers produced during pilot-scale spinning trials underwent thorough characterization by both UVA and Solvay. These fibers consist of well-aligned fibrils bolstered by a matrix, suggesting potential for impressive tensile strength, assuming this reinforcement translates to the carbonized fiber stage. However, the diameters of these fibers are considerably larger than precursor fibers typically resulting in high-strength CF. Refining the material blends and optimizing spinning conditions should enable fiber diameters comparable to those in commercially available CFs. Such adjustments are essential to comprehending the actual tensile capabilities of these fibers.

Nevertheless, the pilot-scale precursor blend fibers produced were converted into CFs at lab-scale. The carbonized fibers do not show any significant void formation or obvious defects at this length scale which indicates that both materials in the blend were able to successfully carbonize simultaneously with sufficient compatibility. The mechanical properties of the CFs were assessed using single-filament tensile testing, yielding an approximate tensile strength of ~1.2 GPa and a tensile modulus of ~100 GPa. These properties stand out despite the carbonized fibers' larger diameters (~40 μm). Significantly reducing the fiber diameter promises to greatly enhance the tensile performance. The blended fibers' crystallinity was also analyzed via XRD and compared with other materials. While exact microstructural parameters are not provided here, the pure high-char polymer displays a crystallite size and distribution akin to PAN – a strong indication that with more precise spinning, drawing, and winding processes leading to diameter reduction this material could yield high tensile strength CFs. Presently, the production of the high-char polymer feedstock is in the initial stages of scale-up, resulting in limited material availability during this project. However, quantities in the kilogram range (> 100 kg) are anticipated to be accessible in 2024. With more time to generate larger material quantities, the team envisions the potential for producing precursor fibers with finer diameters, thus enabling the conversion into CFs possessing significantly elevated tensile modulus and tensile strength.

Milestone 1.4 – Tank performance and cost projection

CF production cost projection

Limited information is available to project the cost of mesophase pitch-derived CF production due to the highly proprietary and protected nature of their production. Therefore, the project team utilized available literature to develop a cost model for the prototype mesophase-pitch derived CF developed by the team. Cost projections for mesophase pitch-derived CF and the proprietary high-char polymer + reactive filler are also provided to offer some perspective of the potential of this novel precursor. The high char polymer + reactive filler is further differentiated into a cost based on current limited feedstock production volume, and a projected cost based on scaled up feedstock production. The results of this modeling are broken down in Figure 9, which includes a cost breakdown for PAN-derived CF production for comparison. Each of the precursors require similar conversion steps including polymerization, spinning, oxidation, carbonization, and post-treatment. The largest differences in cost between the various CF types come from polymerization and spinning. For example, PAN is produced through solution or suspension-based polymerization of acrylonitrile monomers, whereas mesophase pitch is produced from isotropic pitch through a chemically-catalyzed heat treatment process. These processes have fundamentally different requirements, and therefore have different costs associated with them. Furthermore, the productivity of each precursor, as expressed by char yield, varies greatly. The char yield of mesophase pitch and the Solvay high-char polymer + reactive filler are significantly higher than that of PAN. This means that a greater volume of PAN is required to achieve the same amount of CF as the candidate precursors, so the polymerization cost in the model is higher.

The biggest cost advantage of the team’s candidate precursors is due to the application of melt-spinning. PAN precursor fibers must be wet spun, which is expensive due to low throughput, extensive solvent use and recovery, and high capital intensity due to the large

space required for the many successive solvent extraction baths used in this process. Alternatively, melt spinning offers very high throughput, does not require any solvents to achieve suitable precursor fibers, and can be implemented in a much smaller footprint because no coagulation baths are required. The advantages inherent in melt-spinning can be realized for both mesophase pitch and Solvay's proprietary high-char precursor. Not captured in the cost model is a predicted 30% reduction in global warming potential offered by these melt-spinnable precursors compared to PAN. Based on available data, the cost of oxidizing and carbonizing pitch precursor fibers will be equivalent to PAN oxidation and carbonization, and it is predicted that the cost of oxidizing the high-char polymer will be less.

Accordingly, PAN-derived CF is modeled to cost $24.42 / kg CF, and the team's mesophase pitch-derived CF will cost 40% less at $14.69 / kg CF in 2016-year USD. Based on contemporary production levels of the Solvay high-char precursor and reactive filler, these CF will cost $28.90 / kg CF. However, noteworthy cost reductions related to the melt-spinnable polymer can be realized through slight modifications to both the polymer and its polymerization process, which are projected to yield a 65% reduction in raw material expenses, bringing the projected CF manufacturing cost of $16.4/kg. Substantial quantities are expected to be available in 2024 for subsequent spinning, stabilization, and carbonization trials.

Table 2. Carbon fiber cost model results.

Cost ($/kg CF)	Polyacrylonitrile [5,43]	Mesophase Pitch [5,44]	Solvay Blend (Current)	Solvay Blend (Projected)
Polymerization	8.71	3.15	18.5	6
Spinning	4.59	0.42	0.42	0.42
Oxidation	4.58	4.58	4.58	4.58
Carbonization	3.8	3.8	2.66	2.66
Post-treatment	2.74	2.74	2.74	2.74
Total cost	24.42	14.69	28.9	16.4

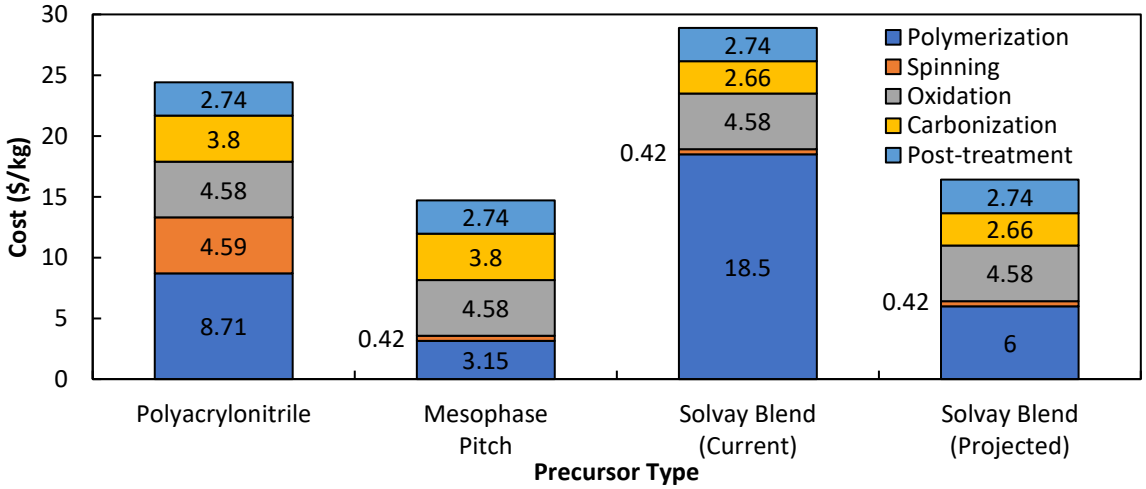

Figure 9. Bar chart of the variable cost estimates from the table above, showing the cost breakdown for each part of the process. Note: Costs are adjusted for 2016.

Tank composite design and modeling

Hexagon designed a Type IV hydrogen storage tank to the HGV2 standard utilizing the CF created by the project team. The tank features a polyamide (PA) liner overwrapped with a mesophase pitch-derived CF/epoxy composite, polyurethane (PU) foam drop protection guards, and aluminum end bosses, Figure 10.

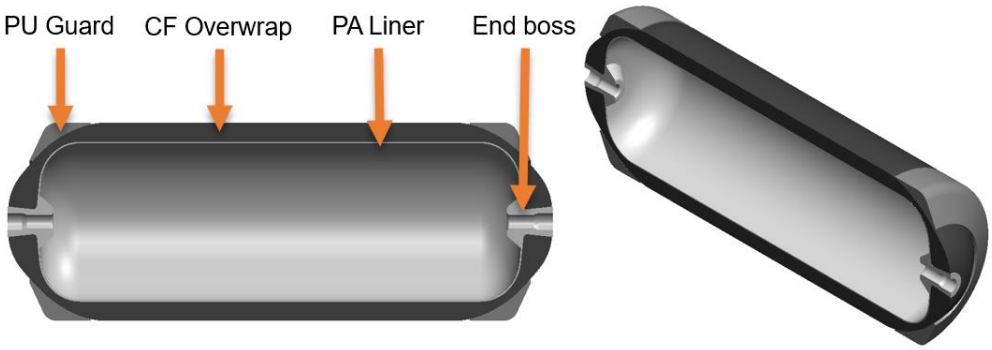

Figure 10. Computer-aided design rendering of the model compressed hydrogen storage tank constructed using the primary candidate CF developed during this project.

The tank performance was modeled using the extensional modulus measured during single filament testing conducted at UVA, and transverse mechanical properties were assumed to be equivalent to typical CF. A Hexagon proprietary epoxy resin was used for the mechanical properties of the matrix. A micromechanics method was used to convert the fiber and resin properties to composite properties using a typical fiber and void volume fraction. The liner thickness was chosen based on internal design standards, and the liner diameter was set to match the DOE required interior diameter.

The composite structure was designed to achieve stress levels in the composite consistent with the fiber strength measured by UVA, a 2.25 stress ratio for CF per the HGV2 standard, and additional design margin based on internal design standards. These stress levels were validated with a finite element model.

Finally, the length of the design was adjusted to achieve the internal DOE required usable storage capacity of 5.6 kg of hydrogen. The physical parameters of the tank are listed in Table 3. With a total mass of 153.1 kg and assuming a hydrogen energy storage capacity of 33.31 kWh/kg H_2, the prototype tank would achieve a gravimetric efficiency of 1.17 kWh/kg. Load transfer efficiency improvements from the team's nanoparticle coating method were not included in the tank performance modeling due to the challenges with the ASTM ring burst testing results.

Table 3. Physical parameters of the prototype tank modeled by Hexagon.

Tank Properties	Value
Exterior Diameter (mm)	500
Exterior Length (mm)	1380
Shell Thickness (mm)	48.24
Total Mass (kg)	131.1
Boss Mass (kg)	2
Liner Mass (kg)	6.6
Composite Mass (kg)	122.5
Stored Mass (kg H_2)	5.8

Tank cost projection

A cost model was developed by Hexagon based on the project downselect guidelines using 2016 currency rates and their proprietary cost modeling methods. The model assumptions and resulting cost projection are shown in Table 4 and Table 5, respectively.

Table 4. Tank cost model assumptions based on 2016 currency rates.

Does not include	Includes
• Profit	• All parameters to meet CSA/ANSI HGV2 standard
• SG&A	• 100,000 units/year factory (incl. all process equipment)
• Capital Depreciation	• Vessel manufacture from CF and general purpose epoxy resin
• Fiberglass protection layer	• PA liner, aluminum bosses, foam domes
	• BOP data supplied by DoE
	• Valve & regulator data provided by DoE
	• Processing Costs
	○ Labor rate: $59,000 / year
	○ Winding, curing, assembly + 10% for investment (incremental cost of larger tank thickness due to lower CF strength fiber)
	○ 10% ROI for all components, including tank processing

Table 5. Cost projection for a tank meeting ANSI HGV2 standards and the parameters set out in the project downselection guidelines.

2016 Cost Model Parameters (100,000 Units)	Units	Program Record		UVA (2016)	
		Cost	Mass (kg)	Cost	Mass (kg)
Composite Tank Total Cost and Mass	$	1926	99	1931	131.1
Balance of Plant (BOP)*	$	993	22	993	22
Assembly	$	11		11	
Total Tank Cost =	$	2930		2935	
Total Tank mass =	kg		121		153.1
Tank Cost =	$/kWh	15.71		15.73	
	kg/kWh		0.65		0.82
Gravimetric Efficiency**	kWh/kg		1.47		1.17

**BOP: Integrated in-tank valve ($219 [3 kg]) + Integrated regulator ($288 [3.6 kg]) + Other BOP ($486 [15.4 kg]).*
***Total H_2 stored and energy stored per kg H_2: 5.6kgH_2 (usable), 33.31kWh/kg*

Performance criteria assessment

Mesophase pitch CF production represents a small fraction of global CF production, and domestic commercial producers of mesophase pitch CFs, such as project partner Solvay, are tightly bound by restrictions that make it prohibitively difficult or impossible to use their facilities for projects such as this one. Consequently, the project team was not able to demonstrate the production of a continuous 100 filament tow, 100 m long, of CFs derived from mesophase pitch. However, an extensive search has yielded clear pathways to achieve these continuous tows, and these opportunities are expanded further in the Continued Development Roadmap section below. The project team is confident that the cost-saving potential and rapid progression in mechanical property development of the mesophase pitch-derived CFs produced at lab-scale warrants evaluation considering that scale-up challenges are driven by availability issues rather than technical limitations.

Per the Statement of Project Objectives, the performance of the prototype fibers and tanks modeled by the project team will be scored according to Table 6.

Table 6. CF and tank performance and cost scoring criteria. Note: Costs are adjusted for 2016.

Points	Carbon Fibers			Tank Estimate	
	Strength (ksi)	*Modulus (Msi)*	*Cost ($/kg)*	*Gravimetric Capacity (kWh/kg)*	*Cost ($/kWh)*
-2		< 28	> 28		
-1		30-32			
0	< 600	> 32	25 – 28	< 1.4	> 15
1	600 – 650		20 – 25	1.4 – 1.5	12 – 15
2	650 – 700		15 – 20	> 1.5	10 – 12
3	700 – 750		< 15		< 10
5	750 – 800				
7	> 800				

CF performance score

The properties of the leading candidate CFs developed during this project are compiled in Table 7 below. These values were measured via single-filament tensile testing adhering to ASTM standard C1557, and the associated score is presented.

Table 7. Average properties of the team's mesophase pitch-derived CF fibers, their respective standard deviation, and the resulting score based on the project scoring rubric.

	Average	Standard Deviation	Score
Strength *(ksi)*	365.5	41.6	0
Modulus *(Msi)*	40.74	4.48	0
Cost *($/kg)*	14.69	-	3
		Total	**3**

Tank performance score

The projected tank performance and cost scores yielded a net tank score of 0 points per the downselect guidelines established for this project, Table 8.

Table 8. Scoring for the tank modeled using the CF developed by the team.

	Projected Performance	Score
Cost *($/kWh)*	15.73	0
Gravimetric Capacity *(kWh/kg)*	1.17	0
	Sum * 2	**0**

Total Downselection Score

Table 9. Total scoring for the CF and tank metrics.

Carbon Fiber Scoring			Tank Scoring		Final Score
Strength	*Modulus*	*Cost*	*Projected Cost*	*Gravimetric Capacity*	*CF + 2x Tank Score*
0	**0**	**3**	**0**	**0**	**0+0+3+(0+0)*2 = 3**

Go/No-Go Decision

At the conclusion of the second budget period, the criteria for a "Go" decision were not satisfied, so the project was given a "No-Go" for Phase 2. The sensitive nature of US domestic production of mesophase pitch-derived CF production, at all stages from fiber spinning to carbonization, prevented the team from scaling up the leading candidate carbon fiber to the required 100+ continuous meters of a 100+ filament tow in the allotted time. It was anticipated that scaled production in industrial facilities would improve the quality of the fibers to meet or exceed the fiber performance criteria, but lab-scale production of the fibers could not meet the baseline tensile strength criteria for the fibers. Ultimately, the lab-scale fiber properties resulted in a projected tank gravimetric capacity and cost that earned a score of 0 points in the downselection criteria. Although the candidate fibers demonstrated superior cost performance, the lack of tensile strength in the fibers resulted in a total downselection score of 3 points, which was not enough to warrant a "Go" decision for Phase 2.

Conclusion

The UVA team has successfully demonstrated the production CFs which can be utilized for the production of hydrogen storage tanks. Several alternative options were explored with two materials selected for further exploration. Mesophase pitch based CFs and a blend of mesophase pitch and Solvay's polymer. Both have shown great promise in terms of mechanical properties and the ability to decrease the cost and global effect with their production as compared to PAN. UVA has also provided a method to increase interfacial shear strength resulting in lower amounts of CF to be required in the composites production and thus decreasing the overall price. Finally, Hexagon has completed the type IV tank design and cost modeling using the produced CFs properties. All factors have resulted in a decreased cost which scored 3 points according to the downselection criteria given.

Publications

1. K.R. Brown, C. Love-Baker, Z. Xue, X. Li, Ultra-high molecular weight polyethylene micro-ribbon fibers gel spun using orange terpenes, *Polymer Engineering and Science*, **64**, 4 (2024) 1743-1755. doi.org/10.1002/pen.26656
2. C.A. Love-Baker, T.M. Harrell, F. Vautard, J. Klett, X. Li, Analysis of the turbostratic structures in PAN-based carbon fibers with wide-angle x-ray diffraction, *Carbon*. **224** (2024). doi.org/10.1016/j.carbon.2024.119037
3. A. Sushchenko, A. Scherschel, C. Love-Baker, R. Cordier, T.M. Harrell, K.R. Brown, X. Li, Evaluating consumer 3D printing nozzles as a low cost alternative for mesophase pitch-derived carbon fiber production, *Carbon*, **225** (2024). doi.org/10.1016/j.carbon.2024.119088
4. T.M. Harrell, C. Le, V. Shen, R. Cordier, X. Li, The effect of stretching on polyamide-6: assessment of crystallinity, mechanical properties, and surface roughness, *J. Polym. Res*. **31**, 198 (2024). doi.org/10.1007/s10965-024-04017-0
5. K.R. Brown, Z. Xue, R. Cordier, C. Love-Baker, E.R. Crater, A. Sushchenko, E. Knight, A. Scherschel, M. Price, R.B. Moore, X. Li, 1,4-cineole: a bio-derived solvent for highly stable graphene nanoplatelet suspensions and well-dispersed UHMWPE nanocomposite fibers, *Advanced Composites and Hybrid Materials*, **7**, 160 (2024). doi.org/10.1007/s42114-024-00977-5
6. A. Scherschel, T.M. Harrell, A. Sushchenko, X. Li, Exploration of fibers produced from petroleum based-mesophase pitch and PET blends for carbon fiber production, *J. Polym. Res.* **30**, 351 (2023). doi:10.1007/s10965-023-03731-5.
7. T.M. Harrell, A. Scherschel, C. Love-Baker, A. Tucker, J. Moskowitz, X. Li, Influence of oxygen uptake on pitch carbon fiber, *Small.* 2023, 2303527. doi:10.1002/smll.202303527

8. A. Scherschel, C. Love-Baker, A. Sushchenko, T. Harrell, K. Brown, X. Li, Compatibility of mesophase pitch and linear low-density polyethylene for low-cost carbon fiber. *J. Polym. Res.* **30**, 82 (2023). doi:10.1007/s10965-023-03466-3.
9. T.M. Harrell, C. Love-Baker, K.R. Brown, C.H. Bumgardner, X. Li, Extracting single fiber transverse and shear moduli from off-axis misalignment fiber tensile testing, *Compos. Part A Appl. Sci. Manuf.* **163** (2022). doi:10.1016/j.compositesa.2022.107204.
10. K.R. Brown, T.M. Harrell, L. Skrzypczak, A. Scherschel, H.F. Wu, X. Li, Carbon fibers derived from commodity polymers: A review, *Carbon*. **196** (2022) 422–439. doi:10.1016/J.CARBON.2022.05.005.
11. K.R. Brown, C. Love-Baker, T.M. Harrell, X. Li, Effect of tension during sulfonation stabilization for UHMWPE-derived carbon fibers, *Journal of Polymer Research*. **30**, 12 (2023) 1-14. doi.org/10.1007/s10965-023-03829-w
12. A. Scherschel, T.M. Harrell, A. Sushchenko, E. Knight, K.R. Brown, X. Li, Tuning microstructure of mesophase pitch carbon fiber by altering the carbonization ramp rate, *Advanced Engineering Materials*. **26**, 12 (2024). doi.org/10.1002/adem.202400110
13. K.R. Brown, X. Li, Continuous Fiber Bath Treatments at Pilot Scale: A novel testbed system [Poster Presentation], *SAMPE* 2022, Charlotte, NC. doi.org/10.2172/1873213

Inventions

1. X. Li, T. Harrell. (2024). *System and method for displacement and strain detection using color tracking* (PCT/US24/41952). Filed August 12, 2024 by University of Virginia Patent Foundation.

References

[1] The markets: Pressure vessels (2020) : CompositesWorld, CompositesWorld. (2019). https://www.compositesworld.com/articles/the-markets-pressure-vessels (accessed February 7, 2020).
[2] M. Veenstra, Compressed Gas Storage Workshop for Medium and Heavy Duty Transportation, 2020.
[3] S. Satyapal, Plenary Remarks, in: U.S. DOE Hydrog. Progr. Annu. Merit Rev. 2023, Arlington, VA, 2023.
[4] D. Warren, Carbon fiber precursors and conversion, 2016.
[5] D. Choi, H.-S. Kil, S. Lee, Fabrication of low-cost carbon fibers using economical precursors and advanced processing technologies, Carbon. 142 (2019) 610–649. https://doi.org/10.1016/j.carbon.2018.10.028.
[6] J. Liu, X. Chen, D. Liang, Q. Xie, Development of pitch-based carbon fibers: a review, Energy Sources, Part A Recover. Util. Environ. Eff. 00 (2020) 1–21. https://doi.org/10.1080/15567036.2020.1806952.
[7] A. K, S.A. O, Carbon-Carbon Composites – A Review, UPI J. Eng. Technol. 1 (2018) 08–19. https://uniquepubinternational.com/journals/index.php/jet/article/view/57 (accessed September 5, 2023).
[8] X. Yin, L. Han, H. Liu, N. Li, Q. Song, Q. Fu, Y. Zhang, H. Li, Recent Progress in 1D Nanostructures Reinforced Carbon/Carbon Composites, Adv. Funct. Mater. 32 (2022) 2204965. https://doi.org/10.1002/ADFM.202204965.
[9] A. Jana, T. Zhu, Y. Wang, J.J. Adams, L.T. Kearney, A.K. Naskar, J.C. Grossman, N. Ferralis, Atoms to fibers: Identifying novel processing methods in the synthesis of pitch-based carbon fibers, Sci. Adv. 8 (2022) 1905. https://doi.org/10.1126/SCIADV.ABN1905.
[10] R. Hufenus, Y. Yan, M. Dauner, T. Kikutani, Melt-spun fibers for textile applications, Materials (Basel). 13 (2020) 1–32. https://doi.org/10.3390/ma13194298.
[11] F. Vautard, J. Dentzer, M. Nardin, J. Schultz, B. Defoort, Influence of surface defects on the tensile strength of carbon fibers, Appl. Surf. Sci. 322 (2014) 185–193. https://doi.org/10.1016/j.apsusc.2014.10.066.
[12] L.T. Drzal, M. Madhukar, Fibre-matrix adhesion and its relationship to composite mechanical properties, J. Mater. Sci. 28 (1993) 569–610. https://doi.org/10.1007/BF01151234.
[13] T.M. Harrell, A. Scherschel, C. Love-Baker, A. Tucker, J.D. Moskowitz, X. Li, Influence of Oxygen Uptake on Pitch Carbon Fiber, Small. 2303527 (2023) 1–10. https://doi.org/10.1002/smll.202303527.

[14] K.R. Brown, T.M. Harrell, L. Skrzypczak, A. Scherschel, H.F. Wu, X. Li, Carbon fibers derived from commodity polymers: A review, Carbon. 196 (2022) 422–439. https://doi.org/10.1016/J.CARBON.2022.05.005.
[15] T. Röding, J. Langer, T.M. Barbosa, M. Bouhrara, T. Gries, A review of polyethylene-based carbon fiber manufacturing, Appl. Res. (2022). https://doi.org/10.1002/APPL.202100013.
[16] D. Zhang, Carbon fibers from oriented polyethylene precursors, J. Thermoplast. Compos. Mater. 6 (1993) 38–48. https://doi.org/10.1177/089270579300600104.
[17] D. Zhang, G.S. Bhat, Carbon fibers from polyethylene-based precursors, Mater. Manuf. Process. 9 (1994) 221–235. https://doi.org/10.1080/10426919408934900.
[18] D. Zhang, Q. Sun, Structure and properties development during the conversion of polyethylene precursors to carbon fibers, J. Appl. Polym. Sci. 62 (1996) 367–373. https://doi.org/10.1002/(SICI)1097-4628(19961010)62:2<367::AID-APP11>3.0.CO;2-Z.
[19] K.R. Brown, C. Love-Baker, T.M. Harrell, X. Li, Effect of tension during sulfonation stabilization for UHMWPE-derived carbon fibers, J. Polym. Res. 2023 3012. 30 (2023) 1–14. https://doi.org/10.1007/S10965-023-03829-W.
[20] C.A. Love-Baker, T.M. Harrell, · Alexander Scherschel, Z. Gao, N. Song, K.R. Brown, F. Vautard, · Ilia Ivanov, J. Klett, · Xiaodong Li, Unveiling the microstructural evolution of carbon fibers derived from polyamide-6, J. Polym. Res. 30 (2023) 1–13. https://doi.org/10.1007/S10965-023-03455-6.
[21] I. Karacan, K.Ş. Tunçel, Thermal stabilization of poly(hexamethylene adipamide) fibers in the presence of ferric chloride prior to carbonization, Polym. Degrad. Stab. 98 (2013) 1869–1881. https://doi.org/10.1016/j.polymdegradstab.2013.05.001.
[22] I. Karacan, H. Meşeli, Characterization of amorphous carbon fibers produced from thermally stabilized polyamide 6 fibers, J. Ind. Text. 47 (2018) 1185–1211. https://doi.org/10.1177/1528083716682922.
[23] I. Karacan, G. Baysal, Investigation of the effect of cupric chloride on thermal stabilization of polyamide 6 as carbon fiber precursor, Fibers Polym. 13 (2012) 864–873. https://doi.org/10.1007/s12221-012-0864-7.
[24] E. Frank, F. Hermanutz, M.R. Buchmeiser, Carbon fibers: Precursors, manufacturing, and properties, Macromol. Mater. Eng. 297 (2012) 493–501. https://doi.org/10.1002/mame.201100406.
[25] T.M. Harrell, C. Le, V. Shen, R. Cordier, X. Li, The effect of stretching on polyamide – 6: assessment of crystallinity, mechanical properties, and surface roughness, J. Polym. Res. 31 (2024) 1–12. https://doi.org/10.1007/s10965-024-04017-0.
[26] A. Scherschel, C. Love-Baker, A. Sushchenko, T. Harrell, K. Brown, X. Li, Compatibility of mesophase pitch and linear low-density polyethylene for low-cost carbon fiber, J. Polym. Res. 30 (2023) 82. https://doi.org/10.1007/s10965-023-03466-3.
[27] A. Scherschel, T. Harrell, A. Sushchenko, X. Li, Exploration of fibers produced from petroleum based-mesophase pitch and pet blends for carbon fiber production, J. Polym. Res. 30 (2023) 1–8. https://doi.org/10.1007/S10965-023-03731-5/METRICS.
[28] A. Dutta, V.M. Nadkarni, Identifying Critical Process Variables in Poly(ethylene Terephthalate) Melt Spinning 1, Text. Res. J. 54 (1984) 35–42. https://doi.org/10.1177/004051758405400108.
[29] A.L. Compere, W.L. Griffith, C.F. Leitten, J.T. Shaffer, Low cost carbon fiber from renewable resources, in: 33rd Int. SAMPE Tech. Conf., Seattle, WA, 2001.
[30] S. Kubo, J.F. Kadla, Lignin-based carbon fibers: Effect of synthetic polymer blending on fiber properties, J. Polym. Environ. 13 (2005) 97–105. https://doi.org/10.1007/s10924-005-2941-0.
[31] E. Svinterikos, I. Zuburtikudis, Carbon nanofibers from renewable bioresources (lignin) and a recycled commodity polymer [poly(ethylene terephthalate)], J. Appl. Polym. Sci. 133 (2016) 1–12. https://doi.org/10.1002/app.43936.
[32] E. Svinterikos, I. Zuburtikudis, M. Al-Marzouqi, The nanoscale dimension determines the carbonization outcome of electrospun lignin/recycled-PET fibers, Chem. Eng. Sci. 202 (2019) 26–35. https://doi.org/10.1016/j.ces.2019.03.013.
[33] C. DiFrancia, T.C. Ward, R.O. Claus, The single-fibre pull-out test. 1: Review and interpretation, Compos. Part A Appl. Sci. Manuf. 27 (1996) 597–612. https://doi.org/10.1016/1359-835X(95)00069-E.
[34] J. Brandstetter, K. Kromp, H. Peterlik, R. Weiss, Effect of surface roughness on friction in fibre-bundle pull-out tests, Compos. Sci. Technol. 65 (2005) 981–988. https://doi.org/10.1016/j.compscitech.2004.11.004.

[35] S. Sockalingam, M. Dey, J.W. Gillespie, M. Keefe, Finite element analysis of the microdroplet test method using cohesive zone model of the fiber/matrix interface, Compos. Part A Appl. Sci. Manuf. 56 (2014) 239–247. https://doi.org/10.1016/j.compositesa.2013.10.021.
[36] A. Qasem, Y.S. Sallam, H. Hossam Eldien, B.H. Ahangarn, Bond-slip behavior between ultra-high-performance concrete and carbon fiber reinforced polymer bars using a pull-out test and numerical modelling, Constr. Build. Mater. 260 (2020) 119857. https://doi.org/10.1016/j.conbuildmat.2020.119857.
[37] Y. Jia, Z. Chen, W. Yan, A numerical study on carbon nanotube-hybridized carbon fibre pullout, Compos. Sci. Technol. 91 (2014) 38–44. https://doi.org/10.1016/j.compscitech.2013.11.020.
[38] Y.Y. Jia, W. Yan, H.Y. Liu, Numetrical study on carbon fibre pullout using a cohesive zone model, ICCM Int. Conf. Compos. Mater. (2011) 1–6.
[39] K.R. Brown, X. Li, Continuous Fiber Bath Treatments at Pilot Scale: A Novel Testbed System, SAMPE 2022, 5/23-26/2022, Charlotte, NC. (2022). https://doi.org/10.2172/1873213.
[40] C. Wang, J. Li, S. Sun, X. Li, F. Zhao, B. Jiang, Y. Huang, Electrophoretic deposition of graphene oxide on continuous carbon fibers for reinforcement of both tensile and interfacial strength, Compos. Sci. Technol. 135 (2016) 46–53. https://doi.org/10.1016/j.compscitech.2016.07.009.
[41] P.K. Gangineni, S. Yandrapu, S.K. Ghosh, A. Anand, R.K. Prusty, B.C. Ray, Mechanical behavior of Graphene decorated carbon fiber reinforced polymer composites: An assessment of the influence of functional groups, Compos. Part A Appl. Sci. Manuf. 122 (2019) 36–44. https://doi.org/10.1016/j.compositesa.2019.04.017.
[42] S.Y. Huang, G.P. Wu, C.M. Chen, Y. Yang, S.C. Zhang, C.X. Lu, Electrophoretic deposition and thermal annealing of a graphene oxide thin film on carbon fiber surfaces, Carbon. 52 (2013) 613–616. https://doi.org/10.1016/j.carbon.2012.09.062.
[43] D. Warren, Lower Cost Carbon Fiber Precursors, in: U.S. Department of Energy, 2012.
[44] J. Sloan, Coming to carbon fiber: Low-cost mesophase pitch precursor, CompositesWorld. (2016). https://www.compositesworld.com/news/coming-to-carbon-fiber-low-cost-mesophase-pitch-precursor.
[45] Zoltek Technologies, Technical Datasheet ZOLTEK™ PX35 Unidirectional Fabrics, n.d.

Appendix A: System and method for displacement and strain detection using color tracking

Background

An image captured from a camera is typically output to a 3D matrix with red, green, and blue color intensity values. Color tracking algorithms are a particular branch of computer vision that can be used to detect and track specific colors or color patterns in an image or video. The first step in a color tracking algorithm is to identify the colors or color patterns that need to be tracked. The color tracking algorithm used here combines the colors from the different channels to determine an intensity in regard to a specific color. For this case, green was utilized because the cameras of interest have twice as many green filters as others. Therefore, to calculate the green intensity the following equation is implemented on each pixel to convert the 3D matrix to a 2D array of green intensity values.

$$I = g - \alpha r - \alpha b \quad (1)$$

where r, g, b are the intensity values from the red, green, and blue channels, respectively, and α is a removal factor.

Figure 11 shows the colors that are found after performing the color tracking algorithm. Figure 11a,b show the colors for the full range of RGB values. Figure 11c shows the unwrapped version of the colors and Figure 11d,e,f show the resulting colors remaining after running the color tracking algorithm for different removal factors. As can be seen, careful selection of α can lead to a down selection of colors detected in the algorithm.

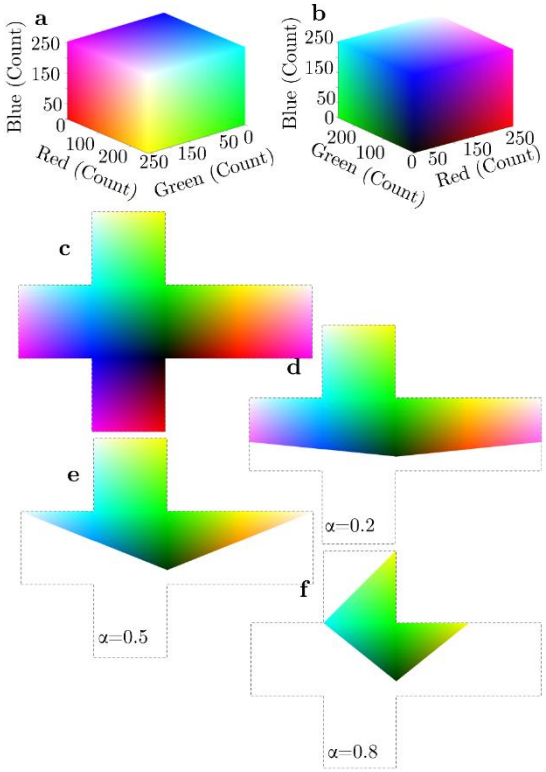

Figure 11. Colors associated with different RGB values for view at the (a) white and (b) dark intensity values. Unwrapped RGB colors (c) on the maximum surface of the RGB values. The reduced color values thresholded using the color tracking algorithm for a reduction (d) 0.2, (e) 0.5, and (f) 0.8.

Experimental methods

Equipment

The color tracking experiments were captured using a Google Pixel 2 XL. The smartphone is equipped with 2 cameras: a main back facing camera and secondary front facing camera. The back facing camera is a 12.2 MP, f/1.8, 27mm wide, 1/2.55", 1.4µm sensor size, dual pixel PDAF, Laser AF, OIS camera and is the only one used for this study. When in video mode the camera specification changes to 4K at 30fps, 1080p at 30/60/120 frames per second (fps), or 720p at 240fps.

Each experiment here was captured in video mode varying 30 frames per second to120 fps. The videos captured were processed with the

phone's software. The resulting video files were then transferred to a computer for further analysis.

Color tracking algorithm

A custom script was created in MATLAB 2022b to perform the color tracking. The script starts by importing the video and extracting an image from the desired frame. The image is then separated into the red, green, and blue channels. The intensities of the green values are calculated via equation (1). To determine the appropriate removal factor, α, and threshold value, T, a small parametric study was performed to assess the effect as shown in Figure 12. Using an α too small results in too many pixels being selected (Figure 12bc) and too high of an α results in less of the object identified (Figure 12e). For this study, α was set to 0.6 based on these results and not changed.

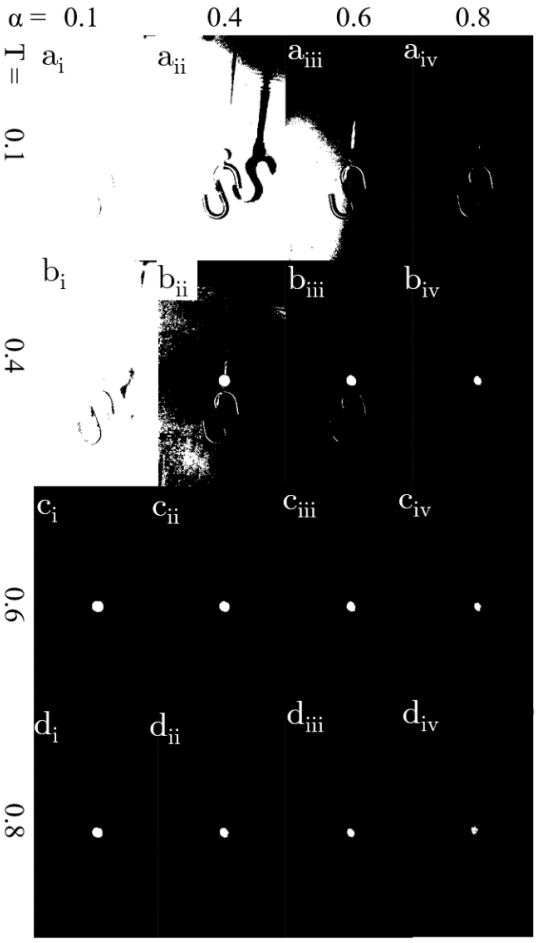

Figure 12. A study on the change in the removal factor, α, and threshold values, T, where the threshold values are (a) T=0.1, (b) T=0.4, (c) T=0.6, (d) T=0.8, and the removal factor changes are denoted with subscripts with (i) being α =0.1, (ii) α =0.4, (iii) α =0.6, and (iv) α =0.8.

Figure 12 shows the results of changing the removal factor and the threshold value. As expected, increasing the removal factor and threshold closer to 1 allows for a more defined selection. The lowest removal factor of 0.1 (Figure 12a_i-a_{iv}) includes features that are not anticipated even with the highest threshold. Increasing the removal factor to 0.4 (Figure 12b_i-b_{iv}) shows the effect of the thresholding value. As the threshold value increases at α=0.4, the selection become closer to only selecting the green dot from the image. Then increasing the removal factor more (Figure 12c_i-c_{iv}) makes the selection more precise. However, overdoing the removal factor (Figure 12d_i-d_{iv}) leaves less of the green marker in the image and therefore less pixels to find the centroid.

Careful selection of the removal factor and the threshold value leaves only the green dot. The script then finds the centroid of the dots by using the 'regionprops' function implemented in MATLAB. This function finds so called regions from a binary image and determines the area and centroid of that region. The region results are sorted from largest to smallest. The first entries that are selected typically correspond to the number of dots used within the experiment. For one dot, there is no further refinement needed and the centroid of the data is found for the dot in all frames. For multiple dots, the full region is sorted by area and down-selected to only the number of dots in the images. Using multiple dots can allow for more complex measurements such as strain or angles. For strain measurements, the initial frame (or multiple zero-strain frames) is used to calculate an

original length. Afterwards, the change in length is calculated for each frame and divided by the original length to calculate strain data.

Displacement and Strain Resolution

The displacement resolution was determined by taking a video of one fiducial marker on a stationary wall. A video was taken from the camera for ~1 minute at 30 fps capturing 1800 images. In addition, the stand-off distance was varied from 10 to 250 cm to determine the change as the field of view (FOV) became larger. The images were then processed using the proposed algorithm to determine the centroid of the fiducial marker.

Figure 13a presents an image at a 10 cm stand-off distance. Figure 13b shows the experimental measurements overlaid on the first frame. The blue circles indicate the centroids extracted from the experiment; the dashed line shows a circle that shows the maximum distance from the average centroid. Figure 13b shows that the proposed method has subpixel resolution. Using the experimental data, the Figure 13c establishes the average pixel noise at each stand-off distance. The pixel noise is determined by taking the average distance from the centroid and is shown as both physical and pixel units. As can be seen the average pixel noise grows as stand-off distance increases but then drops. This may be due to less pixels being available for the centroid to generate noise.

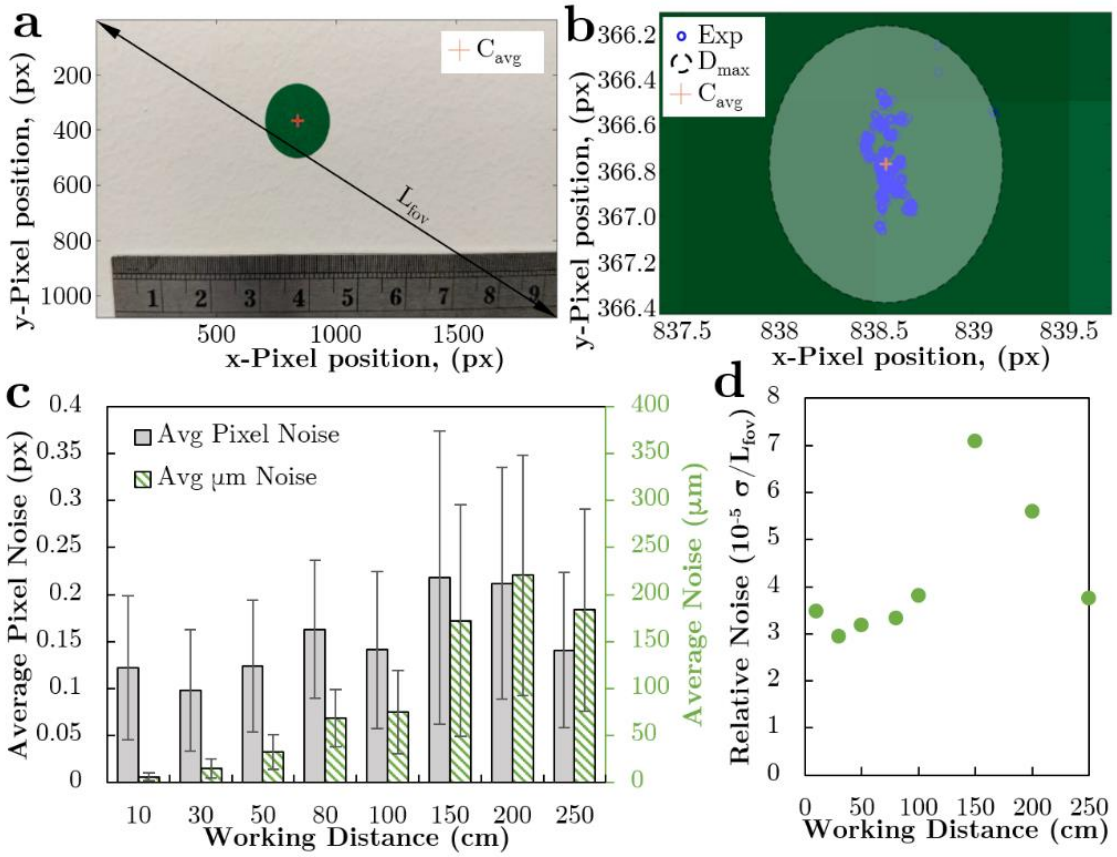

Figure 13. Displacement resolution experiment with (a) showing the full image and (b) showing a image zoomed into close to the centroid where L_{fov} is the diagonal length of the field of view, C_{avg} is the average position of the centroid, Exp is the experimental measurements, D_{max} is the maximum distance from the average centroid. The displacement strain results showing the (c) average noise in pixel and physical units and (d) relative noise.

However, the physical distance shows that even though the noise is lower in pixel units the physical units increase as stand-off distance increases. Figure 13d shows the average noise normalized by the length of the FOV, L_{fov}. The relative noise shows the same trend as the average noise.

Since these are point measurements, the strain is related to the gauge length. The strain

$$\varepsilon = \Delta L/L \quad (2)$$

where ΔL is the change in length, and L is the original gauge length.

Applying the noise to the system and assuming that the change in length is zero, results in:

$$\varepsilon = 2\mathrm{N}/L \quad (3)$$

where N is the noise level.

As the gauge length decreases, the noise increases. Therefore, making the strain resolution variable.

Tracking Comparision

Moving Pendulum Experiment

The moving pendulum experiment was conducted as an example of displacement tracking with the higher frame rate (120 fps). A green bead was strung through a tow of nylon fibers that was tied to a weight. The whole system is rigidly moving in an upwards direction until out of the frame. A tow of nylon fibers was tied to an S-hook to act as a weight. A green bead was threaded through the fibers and sat atop of the weight. The fibers were then clamped to an Admet expert universal tensile machine. The weight was moved and released to create a pendulum. The Admet UTM was then jogged in an upward direction at a rate of 100 mm/min. The camera captured the movement of the ball until it proceeded out of frame.

Point tracking with DIC

As a point of comparison, tracking of the point was performed with digital image correlation (DIC) using VIC-2D software. The full image was used as an area of interest. The subsets were varied to contain the most data over the time and provide a compromise between noise and accuracy.

Comparison Results

Figure 14 presents the horizontal and vertical displacements from the proposed color tracking algorithm and the DIC correlation. Figure 14a shows the full displacement time history of both measurements overlayed on the final frame of the video. It shows that the DIC and color tracking measurements were close over the first ~10% of the video, Figure 14b,d. However, the DIC algorithm decorrelated after this point. This is due to the lack of a random speckle pattern on this test and the fact that DIC is developed for small displacements and small strains. Figure 14c,e show the region that the DIC correlated. Over this region, the DIC correlated well and maintained similar measurements with the color tracking algorithm within 5%. However, it was noisier than the color tracking especially near the transitions or the peaks of the wave. The average of the absolute

difference between these two sets of data are 3.08 and 1.14 pixels for the horizontal and vertical displacements, respectively.

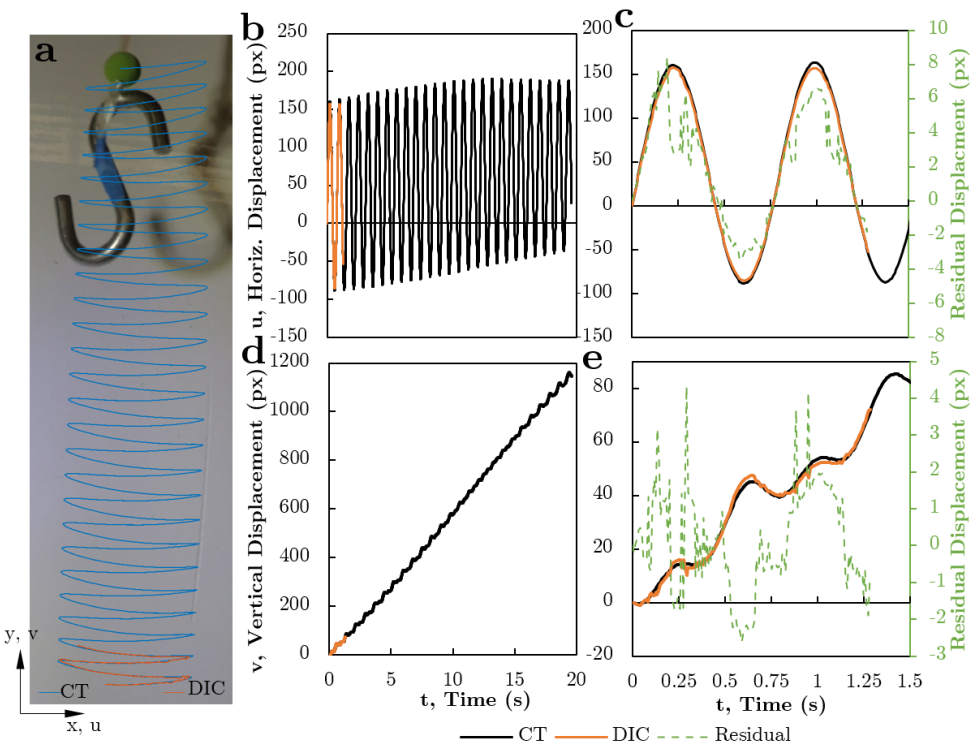

Figure 14. Comparison of DIC measurements to proposed color tracking method where (a) presents the last image of the video overlayed with the displacements determined by the proposed color tracking algorithm and the DIC correlation algorithm. Plots of the horizontal and vertical displacements are shown for the full video in (b,d) and a subset of the video from 0 to 1.5 seconds in (c,e).

Tensile Tests on Carbon Fiber Reinforced Polymer

A tensile test was conducted on a carbon fiber tow specimen to evaluate the performance of the color tracking algorithm in determining strain between two fiducial markers. The ability to track the displacement on the material rather than the grips is vital to truly testing material properties due to inaccuracies with the measurements. These inaccuracies stem from errors such as compliance of the test machine with stiff materials or grip slippage. The tow was made of Zoltek Panex 35 carbon fiber [A1] with West Systems 105 epoxy resin with ~55% volume fraction. The tensile test in accordance to ASTM D4018. The test was recorded at 120 fps frame rate for 35 seconds. Figure 15a shows the experimental setup. Two fiducial markers, green stickers, were placed on the surface of the cured tow. The specimen was subjected to a uniaxial tensile load using an Admet expert universal testing machine 2600, and the displacement and strain were recorded using the color tracking algorithm. Figure 15b shows the stress-strain results. The stress-strain relationship as expected was linear. The calculated modulus closely matched the values reported in the Zoltek material's datasheet [A1]. This demonstrated the ability for the algorithm to accurately capture the strain and displacement even for small displacements.

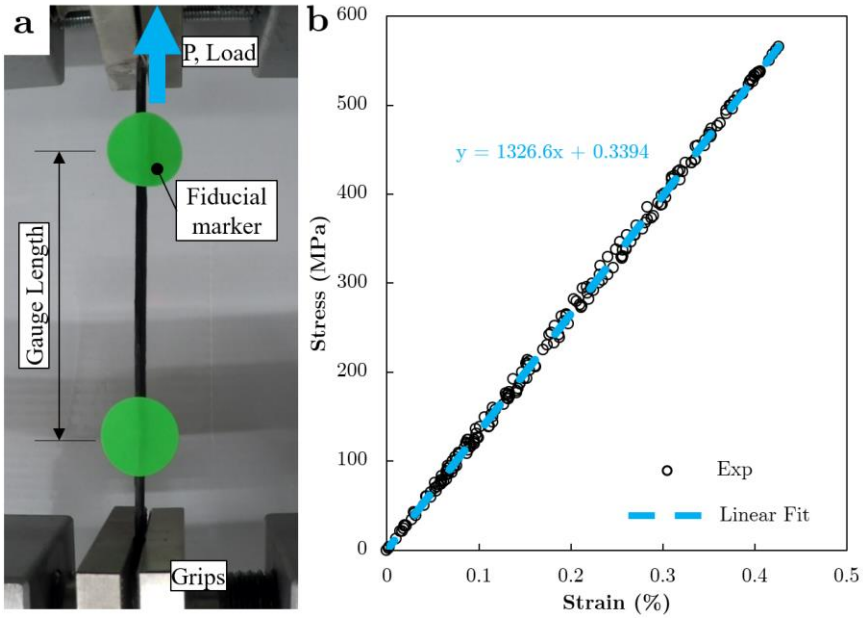

Figure 15. (a) Experimental test setup of the tensile test and (b) results from the tensile test showing the stress and strain relationship

Conclusions

In conclusion, this study presents a novel and cost-effective technique for accurate displacement and strain measurement using a color tracking algorithm. By leveraging the capabilities of a mobile phone camera and a green fiducial marker, the algorithm provides a low-cost alternative to traditional optical measurement methods.

The findings of this study demonstrate the effectiveness of the color tracking algorithm in capturing displacement and strain with higher precision and low noise. The simplicity and affordability of the color tracking algorithm make it an attractive solution for displacement and strain measurement in various fields. The use of a mobile phone camera significantly reduces financial barriers and enhances accessibility. Simplicity and ease of implementation makes this technique a valuable educational tool for students learning about optical measurement techniques. The potential applications of the color tracking algorithm extend beyond material science; Its versatility in capturing motion opens possibilities for its utilization in biomechanics, rehabilitation, and related fields.

Future research directions could focus on expanding the capabilities of the color tracking algorithm to enable full-field measurements and exploring its potential for real-time tracking applications. Additionally, further investigations could explore the algorithm's performance under various lighting conditions and its robustness to different materials and surface characteristics.

Appendix References

[A1] Zoltek Technologies, Technical Datasheet ZOLTEKTM PX35 Unidirectional Fabrics, n.d.